Supplement of Biogeosciences, 17, 5563–5585, 2020
https://doi.org/10.5194/bg-17-5563-2020-supplement

Biogeosciences Open Access EGU

Supplement of

Introduction: Process studies at the air–sea interface after atmospheric deposition in the Mediterranean Sea – objectives and strategy of the PEACETIME oceanographic campaign (May–June 2017)

Cécile Guieu et al.

Correspondence to: Cécile Guieu (guieu@obs-vlfr.fr) and Karine Desboeufs (karine.desboeufs@lisa.u-pec.fr)

This file contents:

- **5 figures (S1 to S5)**
- **1 text section**
- **References**

1. Figures.

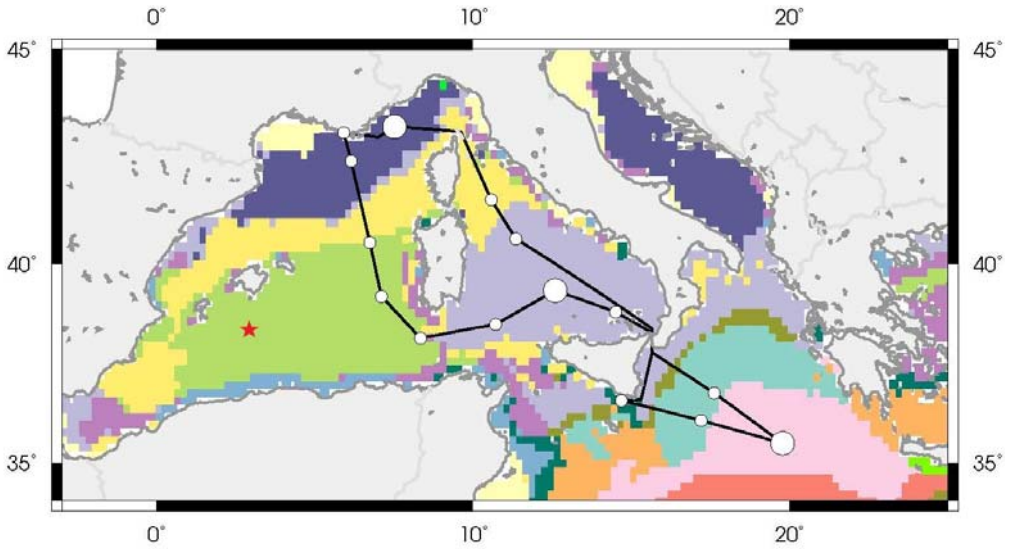

Figure S1. Spatial distribution of the Mediterranean epipelagic marine ecosystems of the Mediterranean Sea. The initially planned transect is superimposed. Each ecoregion detected on that figure presents a characteristic species association from primary producers to top predators of the epipelagic domain, forced by similar environmental conditions (From Reygondeau et al., 2014). (The red star is the position of the station FAST, not initially planned).

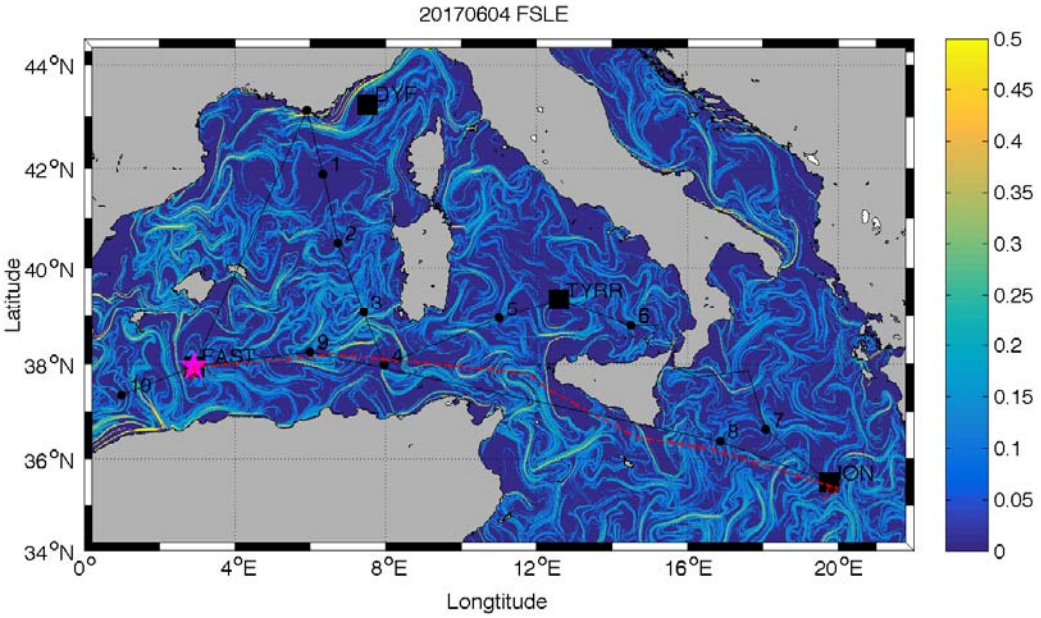

Figure S2. Map of the FSLE (Finite Size Lyapunov Exponent, day-1) calculated from the near-real-time altimetry-derived surface currents for June 4, 2017. The figure is extracted from the SPASSO bulletin of June 5, 2017 with the planned stations shown in black and the route toward the FAST station highlighted in magenta.

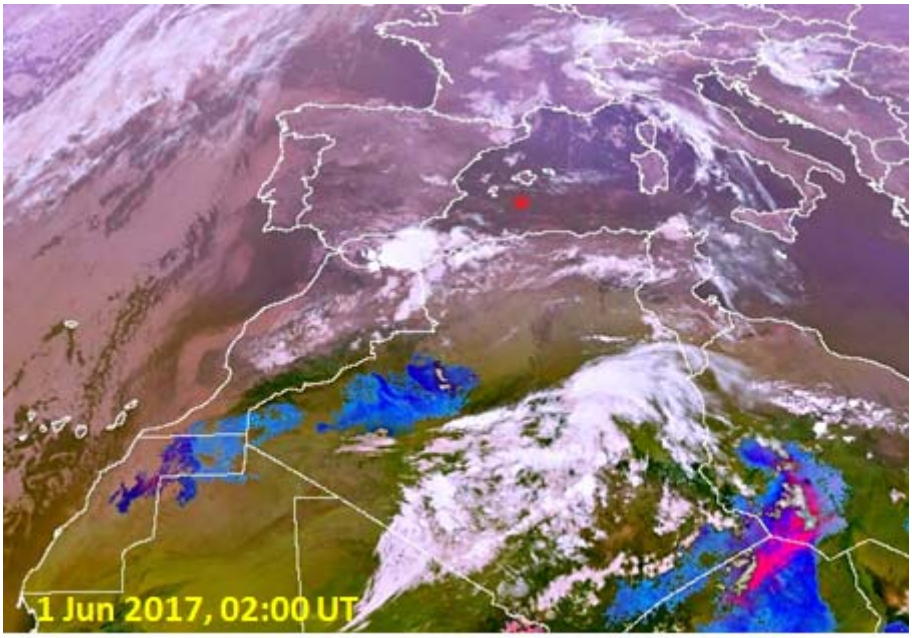

Fig S3. NASCube image window over North Africa and southern Europe for 1 June 2017, 02 UT. This nighttime image was derived from MSG/SEVIRI thermal infrared channels

by comparison to a clear reference image for the period, allowing detection ofng high dust load over the continental surfaces (Legrand et al., 2001). White tones indicate clouds, the highest being the brightest and the thermal anomalies attributable to dust are coloured by increasing intensity from blue to pink. They are associated with increasing AOD from light blue (typically <0.3) to purple (~1) and pink (>2) (Gonzalez and Briottet, 2017). (The red star is the position of the station FAST).

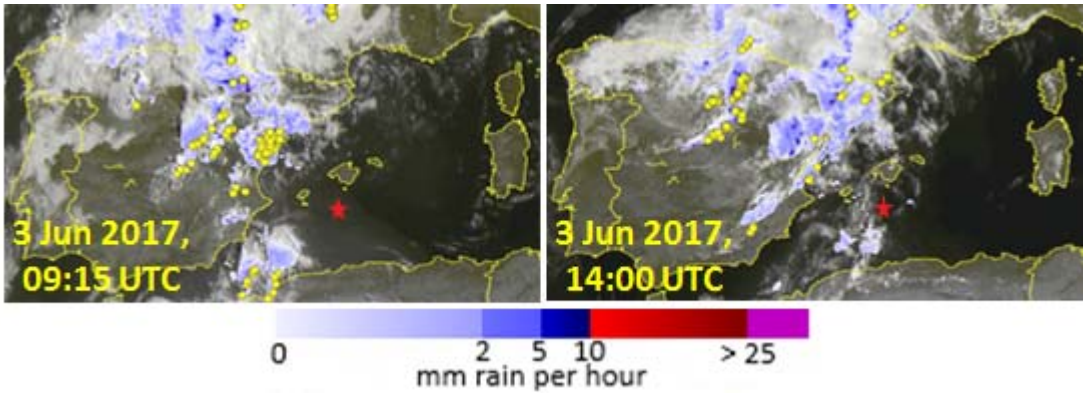

Figure S4. Rain-lightning-clouds (RLC) image window over the western Mediterranean and Spanish Peninsula showing clouds (white areas), estimated precipitation (blue shades), and lightning strikes (yellow circles) obtained by combining SEVIRI infrared images and European rain radars (from meteoradar.co.uk; access 3 June 2017). (The red star is the position of the station FAST).

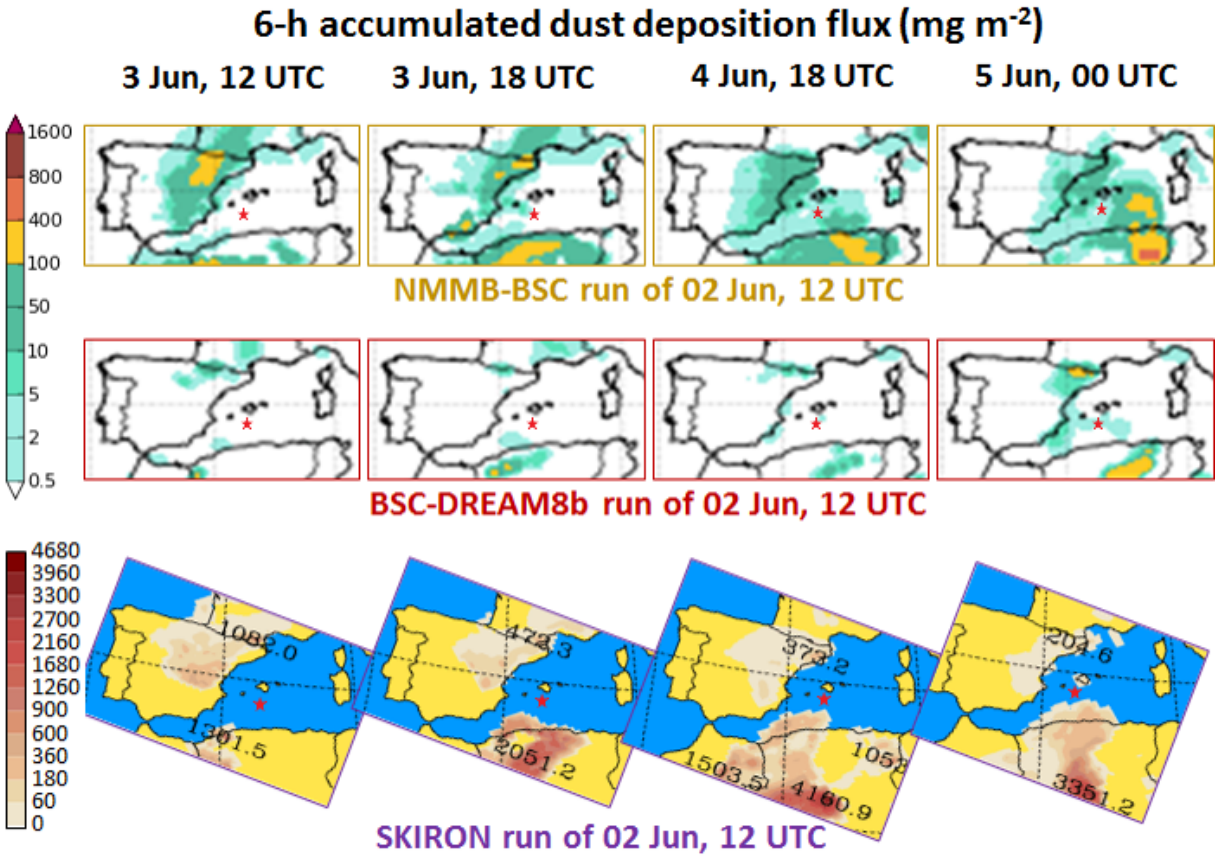

Figure S5. Maps of 6-h accumulated desert dust wet deposition fluxes in the western Mediterranean produced by the forecast run of 2 June 2017 of the three dust transport models NNMB-BSC-Dust-v2 (top) BSC-DREAM8b (middle) and SKIRON (bottom), at times 3 Jun, 12 UTC and 18 UTC, 4 Jun 18 UTC and 5 Jun 00 UTC from left to right, respectively. (The red star is the position of the station FAST).

2. Text.

Tools for decision. Several near-real time remote sensing products and model forecasts were used. In terms of aerosol remote sensing, we mainly relied on two products. The first one was the aerosol optical depth at 550 nm (AOD_{550}) distribution over the sea, as produced in near-real time by the ICARE data and service centre, Lille, France (product SEV_AER-OC-L2;

http://www.icare.univ-lille1.fr/projects/seviri-aerosols; last access 9 June, 2020). Data from the Spinning Enhanced Visible and Infra-red Imager (SEVIRI) on-board the geostationary satellite Meteosat Second Generation (MSG) are directly acquired every 15 min by the Service d'Archivage et de Traitement Météorologique des Observations Satellitaires of the Centre de Météorologie Spatiale (CMS/SATMOS), Lannion, France, and processed within hours by ICARE based on the algorithm of Thieuleux et al. (2005). The MSG satellite position at 0° longitude allows a good coverage for aerosol climatologies and case studies of aerosol transport over the Mediterranean basin (e.g. figure I.19 in Lionello et al., 2012; Chazette et al., 2016 and 2019) and surrounding continental regions (Carrer et al., 2014) as well as of desert dust source regions in Africa (e.g. Gonzales and Briottet, 2017). In addition to the quick-look from the level-2 product (SEV_AER-OC-L2) available between 4:30 and 18:00 UT at the maximum in mid-June in our area of interest, a daily mean level-3 (SEV_AER-OC-D3) is produced every night by averaging all available time slots during the previous day between 4:00 and 19:45 UT. Figure 6 (main text) illustrates this product for the 3rd of June when an African dust plume from North Africa associated to a cloudy air mass invaded the westernmost Mediterranean basin atmosphere. The horizontal resolution of the product is of 3 x 3 km^2 at nadir, of the order of 12.5 km^2 in the Alboran Sea, 15 km^2 in the North of the Gulf of Genova, and 18 km^2 in the northeasternmost basin (about 13.07, 13.64, and 13.96 at the FAST, ION, and TYR station, respectively). Although less accurate than AOD from MODIS when compared to AERONET data, the high temporal resolution of MSG/SEVIRI-derived AOD offers a much better daily coverage of the area than any orbiting satellite (Bréon et al., 2011), especially when partial cloud coverage can be compensated thanks to successive images, as illustrated in figure 6.

The second useful remote sensing product was the North African Sand Storm Survey (NASCube) also produced from MSG/SEVIRI, at the Laboratoire d'Optique Atmosphérique, Lille, France (http://nascube.univ-lille1.fr; last access, 9 June 2020). It generates continuous

day and night images of desert dust plumes over the northern African continent and Arabian Peninsula, using an artificial neural network methodology producing colour composite images by processing 8 visible, near-infrared and thermal infrared bands of SEVIRI (Gonzales and Briottet, 2017). Figure SI-3 shows a window of this product for the 1st June 2017, showing the probable dust source regions (south of Morocco and western Algeria) of the plume found the following days over the westernmost Mediterranean basin as seen in figure 6.

During the campaign, we also used, on a regular basis, air mass trajectories computed with the Hysplit tool of the Air Resources Laboratory of the National Ocean and Atmosphere Administration (NOAA/ARL; https://ready.arl.noaa.gov/HYSPLIT_traj.php; last access 9 June 2020; Stein et al., 2015; Rolph et al., 2017) based on global meteorological 192-h forecasts from the Global Forecasting System (GFS) model (1-deg, 3-h resolution) operated by the National Centers for Environmental Prediction (NCEP; Yang et al., 2006). It could be used both in forward mode to forecast the transport over the western Mediterranean of dust plumes detected over Africa by NASCube, and in backward mode to identify the origin of air masses over the ship position.

In addition to aerosol remote sensing observations, we also used near real time rainfall remote sensing produced by the Meteo Company, an international weather network (https://meteoradar.co.uk; last access 9 June 2020) providing every 15 minutes real time weather radar- and satellite-derived maps of precipitation, clouds, and lightning on a European window covering most of the Mediterranean basin (north of 32°N or 35.5°N, depending on products). The satellite infrared images from SEVIRI are filtered to show the thicker clouds, and observations from 45 European rain radar are integrated. Figure SI-4 illustrates the combined SEVIRI satellite and radar product showing both clouds, precipitation and lightning for two time slots on 3 June 2017. They show the beginning and the end, respectively, of a

convective rainfall of low intensity (<2 mm h-1) between Algeria and Spain in the dusty and cloudy area visible in Figure 6 west of the ship.

A number of operational forecast models were also used, both for weather forecast and aerosol transport. In order to understand the synoptic circulation, we especially considered surface pressure (*P*) and 500-hPa (about 5.5-km altitude) geopotential (*Z500*) maps over the European domain covering the whole Mediterranean basin and northern Atlantic from the global numerical weather prediction model ARPEGE (Courtier and Geleyn, 1988), developed and maintained at Météo-France. Its horizontal resolution varies from 7.5 km in France to 37 km over Southern Pacific, and four daily forecasts including data assimilation are carried out every day (available by http://www.meteociel.fr, last access 9 June 2020). Because we were especially targeting possible aerosol deposition events, we also analysed daily a set of up to 5-days, 1-, 3-, or 6-hourly depending on models, precipitation forecasts from several models including those made available by meteociel.fr including global weather forecast models such as ARPEGE, IFS (the model developed at ECMWF; Barros et al. 1995), the Canadian CMC-MRB GEM model (Côté and Gravel, 1998), the GFS atmospheric model from NCEP (Kanamitsu, 1989) and its ensemble GEFS, but also the regional non-hydrostatic model AROME (Seity et al., 2011) for the NW Mediterranean only at 1.3 km resolution.

Three regional dust transport models have also been considered, namely SKIRON operated by the Atmospheric Modeling and Weather Forecasting Group (AM&WFG) of the University of Athens (Kallos et al., 2009; Spyrou et al., 2010) and the two models NMMB-BSC (Non-Hydrostatic Multiscale Model; Pérez et al., 2011) and BSC-DREAM8b (Basart et et al., 2012) operated by the Barcelona Supercomputing Centre (BSC). SKIRON and BSC-DREAM8b have a horizontal resolution of 0.24° and 0.33°, respectively, and are both initialized and constrained at their boundaries by NCEP/GFS 6-hourly data. NMMB-BSC regional model has a resolution of 0.47° x 1/3° and is constrained by the NCEP global version of the model (Pérez et al., 2011).

In terms of dust transport modeling, we mainly relied on 6-hourly dust optical depth and dry and wet dust deposition fluxes forecasted daily from 12 UTC over the next 72 h by the NMMB-BSC-Dust and BSC-DREAM8b v2.0 models and over the next 180 h (5.5 d) by SKIRON. Because of its longer temporal range of forecast, the wet dust deposition product by SKIRON was particularly useful to issue an early pre-alert for the Fast Action during the cruise. Figure SI-5 compares the forecast maps of 6-h accumulated dust deposition flux at 4 time steps from 3rd June 2017 12 UTC to 5 June 00 UTC, from the 2nd June runs of those 3 models. This period corresponds to the scavenging of the dust plume shown in Figure 6 that was targeted for the Fast Action (see below).

We also used a set of forecast of aerosol or dust optical depth from a series of models: (i) 60-h, 6-hourly ensemble and comparative forecasts of dust optical depth from models operated by the BSC for the World Meteorological Organization (WMO) Sand and Dust Storm Warning Advisory and Assessment System (SDS-WAS), and made available by the Spanish Agencia Estatal de Meteorologia (AEMET; https://sds-was.aemet.es/forecast-products/dust-forecasts/; last access 9 June 2020; it is worth noting that Basart et al. (2016) model data comparison over summer 2012 showed better average performances of the model ensemble dust forecasts compared to forecasts from any individual model (ii) 5-days, 3-hourly dust and sulphate AOD Copernicus/GMES products over Europe and North Africa produced by the European Center for Medium-Range Forecast (ECMWF), and (iii) 114-h, 6-hourly sulfate, dust and smoke AOD over Europe and the Mediterranean region north of 35°N from the Naval Research Laboratory (NRL) global NRL Aerosol Analysis and Prediction System (NAAPS) model that is using an AOD assimilation package (Zhang et al., 2008); further, we used the kml formatted animations of the NAAPS 5-days global forecasts of AOD projected on a GoogleEarth satellite view centered on the western Mediterranean, which shows areas with significant AOD (>0.1) of sulfate, dust or smoke. Finally, we also considered the daily maps (at time 00 UTC) produced

by the Earth Wind Map community (https://earth.nullschool.net; last access 9 June 2020), consisting of AOD from sulfate or dust from the NASA Global Modeling and Assimilation Office (GMAO) Goddard Earth Observing System version 5 (GEOS-5) model overlaid by surface or 700 hPa winds from the GFS model in order to check the dominant aerosol type and transport conditions at the ship position.

3. References

1. Barros, S.R.M., Dent, D., Isaksen, L., Robinson, G., Mozdzynski, G., & Wollenweber, F. (1995) The IFS model: A parallel production weather code, Parallel Computing, 21, 1621-1638, doi:10.1016/0167-8191(96)80002-0.
2. Basart S., F. Dulac, J.M. Baldasano, P. Nabat, M. Mallet, F. Solmon, B. Laurent, J. Vincent, L. Menut, L. El Amraoui, B. Sic, J.-P. Chaboureau, J.-F. Léon, K. Schepanski, J.-B. Renard, F. Ravetta, J. Pelon, C. Di Biagio, P. Formenti, I. Chiapello, J.-L. Roujean, X. Ceamanos, D. Carrer, M. Sicard, H. Delbarre, G. Roberts, W. Junkermann, & J.-L. Attié (2016) Extensive comparison between a set of European dust regional models and observations in the western Mediterranean for the summer 2012 pre-ChArMEx/TRAQA campaign, In Air Pollution Modeling and its Application XXIV, D.G. Steyn and N. Chaumerliac Eds., Springer Series Proc. in Complexity, 79-83, doi:10.1007/978-3-319-24478-5_13.
3. Basart S., Pérez, C., Nickovic, S., & Baldasano, J.M. (2012) Development and evaluation of the BSC-DREAM8b dust regional model over Northern Africa, the Mediterranean and the Middle East, Tellus, 64, 18539, doi:10.3402/tellusb.v64i0.18539.
4. Bréon, F.-M., Vermeulen, A., & Descloitres, J. (2011) An evaluation of satellite aerosol products against sunphotometer measurements, Remote Sensing of Environment, 115, 3102-3111, doi:10.1016/j.rse.2011.06.017.
5. Carrer D., X. Ceamanos, B. Six, & J.-L. Roujean (2014) AERUS-GEO: A newly available satellite-derived aerosol optical depth product over Europe and Africa, Geophysical Research Letters, 41, 7731-7738, doi:10.1002/2014GL061707.
6. Chazette, P., Totems, J., & Shang, X. (2019) Transport of aerosols over the French Riviera – link between ground-based lidar and spaceborne observations, Atmospheric Chemistry and Physics, 19, 3885–3904, doi:10.5194/acp-19-3885-2019.
7. Chazette, P., Totems, J., Ancellet, G., Pelon, J., & Sicard, M. (2016) Temporal consistency of lidar observations during aerosol transport events in the framework of the ChArMEx/ADRIMED campaign at Minorca in June 2013, Atmospheric Chemistry and Physics, 16, 2863–2875, doi:10.5194/acp-16-2863-2016.
8. Côté, J., S. Gravel, A. Méthot, A. Patoine, M. Roch, & A. Staniforth, 1998: The Operational CMC–MRB Global Environmental Multiscale (GEM) Model. Part I: Design Considerations and Formulation. Mon. Wea. Rev., 126, 1373–1395, doi:10.1175/1520-0493(1998)126<1373:TOCMGE>2.0.CO;2.

9. Courtier, P. & Geleyn, J.-F. (1988) A global numerical weather predic-tion model with variable resolution: Application to the shallowmodel equations, Q. J. Roy. Meteor. Soc., 114, 1321–1346, doi:10.1002/qj.49711448309.
10. Gonzales, L., & Briottet, X (2017) North Africa and Saudi Arabia day/night sandstorm survey (NASCube), Remote Sensing, 9, 896, doi:10.3390/rs9090896.
11. Kallos, G., Spyrou, C., Astitha, M., Mitsakou, C., Solomos, S., Kushta, J., Pytharoulis, I., Katsafados, P., Mavromatidis, E., Papantoniou, N., & Vlastou, G. (2009) Ten-year operational dust forecasting - Recent model development and future plans. WMO/GEO Expert Meeting on an International Sand and Dust Storm Warning System, IOP Conference Series: Earth and Environmental Science, 7, 012012, doi:10.1088/1755-1307/7/1/012012.
12. Kanamitsu, M. (1989) Description of the NMC global data assimilation and forecast system, Weather and Forecasting, 4, 335-342, doi:10.1175/1520-0434(1989)004<0335:DOTNGD>2.0.CO;2.
13. Legrand, M., Plana-Fattori, A., & N'doumé, C. (2001) Satellite detection of dust using the IR imagery of Meteosat: 1. Infrared difference dust index, Journal of Geophysical Research: Atmospheres, 106, 18251-18274, doi:10.1029/2000JD900749.
14. Lionello P., Abrantes, F., Congedi, L., Dulac, F., Gacic, M., Gomiz, D., Goodess, C., Hoff, H., Kutiel, H., Luterbacher, J., Planton, S., Reale, M., Schröder, K., Struglia, M.V., Toreti, A., Tsimplis, M., Ulbrich, U., & Xoplaki, E. (2012) Introduction: Mediterranean climate–Background information, In The Climate of the Mediterranean Region: From the Past to the Future, P. Lionello Ed., Elsevier, pp. xxxv-xc, doi:10.1016/B978-0-12-416042-2.00012-4.
15. Pérez, C., Haustein, K. Janjic, Z. Jorba, O., Huneeus, N., Baldasano, J.M., Black, T., Basart, S., Nickovic, S., Miller, R.L., Perlwitz, J.P., Schulz, M., & Thomson, M. (2011) Atmospheric dust modeling from meso to global scales with the online NMMB/BSC-Dust model - Part 1: Model description, annual simulations and evaluation, Atmospheric Chemistry and Physics, 11, 13001-13027, doi:10.5194/acp-11-13001-2011.
16. Reygondeau, G., Irisson, J.-O., Ayata, S., Gasparini, S., Benedetti, F., Albouy, C., Hattab, T., Guieu, C., Koubbi, P. (2014) Definition of the Mediterranean eco-regions and maps of potential pressures in these eco-regions. Technical Report. Deliverable Nr. 1.6. FP7-PERSEUS project.
17. Rolph, G., Stein, A., & Stunder, B. (2017) Real-time Environmental Applications and Display sYstem: READY, Environmental Modelling & Software, 95, 210-228, doi:10.1016/j.envsoft.2017.06.025.
18. Seity, Y., Brousseau, P., Malardel, S., Hello, G., Bénard, P., Bouttier,F., Lac, C., and Masson, V.: The AROME-France Convective-Scale Operational Model, Mon. Weather Rev., 139, 976–991,https://doi.org/10.1175/2010MWR3425.1, 2011
19. Spyrou, C., Mitsakou, C., Kallos, G., Louka, P., & Vlastou, G. (2010) An improved limited area model for describing the dust cycle in the atmosphere, Journal of Geophysical Research: Atmospheres, 115, D17211, doi:10.1029/2009JD013682.
20. Stein, A.F., Draxler, R.R, Rolph, G.D., Stunder, B.J.B., Cohen, M.D., & Ngan, F. (2015) NOAA's HYSPLIT atmospheric transport and dispersion modeling system, Bull. Amer. Meteor. Soc., 96, 2059-2077, doi:10.1175/BAMS-D-14-00110.1.

21. Thieuleux, F., Moulin, C., Bréon, F. M., Maignan, F., Poitou, J., & Tanré, D. (2005) Remote sensing of aerosols over the oceans using MSG/SEVIRI imagery, Annales Geophysicae, 23, 3561–3568, doi:10.5194/angeo-23-3561-2005.
22. Yang, F., Pan, H.-L., Krueger, S.K., Moorthi, S., & Lord, S.J. (2006) Evaluation of the NCEP global forecast system at the ARM SGP site, Monthly Weather Review, 134, 3668-3690, doi:10.1175/MWR3264.1.
23. Zhang, J., Reid, J.S., Westphal, D.L., Baker, N.L., & Hyer, E.J. (2008) A system for operational aerosol optical depth data assimilation over global oceans, Journal of Geophysical Research: Atmospheres, 113, D10208, doi:10.1029/2007JD009065.